Available online at www.sciencedirect.com

SciVerse ScienceDirect

Ceramics International 39 (2013) 6251–6263

CERAMICS INTERNATIONAL

www.elsevier.com/locate/ceramint

On the determination of the film hardness in hard film/substrate composites using depth-sensing indentation

N.A. Sakharova[a,*], M.C. Oliveira[a], J.M. Antunes[b], J.V. Fernandes[a]

[a]CEMUC-Department of Mechanical Engineering, University of Coimbra, Rua Luís Reis Santos, Pinhal de Marrocos, 3030–788 Coimbra, Portugal
[b]Escola Superior de Tecnologia de Abrantes, Instituto Politécnico de Tomar, Rua 17 de Agosto de 1808, 2200 Abrantes, Portugal

Received 30 October 2012; received in revised form 28 December 2012; accepted 12 January 2013
Available online 29 January 2013

Abstract

The main difficulty in the mechanical characterisation of thin films using depth-sensing indentation is the determination of the relative substrate and film contributions to the measured properties of the film/substrate composite. In this study, a three-dimensional numerical simulation of the Vickers hardness test is used to study the influence of the substrate and film mechanical properties on the composite's behaviour under depth-sensing indentation. The particular case of hard films on soft substrates is analysed. In order to understand the behaviour of the composite, a study of the plastic strain distribution under indentation of several composites is performed. A methodology to determine the relative film hardness, i.e. H_F/H_S ratio, is proposed. The methodology is successfully verified using fictitious and real composite materials.

Keywords: B. Composites; C. Hardness; Vickers indentation; Numerical simulation

1. Introduction

Hardness is one of the most important mechanical properties in the mechanical characterisation of materials. The depth-sensing indentation technique is commonly used for evaluation of the hardness of bulk and coating materials. In the case of thin coatings, elastic and plastic deformations can occur in the film and the substrate, during the hardness test. Therefore, the main difficulty in evaluating film hardness is to distinguish the contribution of the substrate from that of the film and the measured composite hardness, H_C, depends on the film and substrate hardness, H_F and H_S, respectively. This is especially so for small thicknesses and/or when the ratio between the film and substrate hardness (H_F/H_S) is very different from unity [1]. Consequently, for the maximum indentation depths commonly used in experimental tests, the composite hardness, H_C, is a function of the film and substrate mechanical properties. In this context, the composite hardness depends on the maximum applied load or, as usually expressed, on the relative contact indentation depth, h_c/t, *i.e.* the ratio between the contact indentation depth, h_c, and the film thickness, t.

In some applications, the film thickness can be lower than ten nanometres. In these cases, low indentation depths are required for determining film hardness, since the plastic response of the composite can significantly deviate from that of the film, for indentation depths of only around 10 to 15% of the film thickness (see, for example, [2,3]). As previously stated, the critical indentation depth depends on the film and substrate mechanical properties, namely hardness (or yield stress) and Young's modulus ratios [1,4]. Moreover, in an investigation [5] on the critical indentation depth rule, according to which the substrate has a negligible effect on the composite hardness, divergences were found. These authors established that the critical indentation depth is sensitive to film structure (crystal, polycrystalline or amorphous), which determines the plastic deformation mechanisms and, consequently, the size of the region under the indenter that suffers from plastic strain. This shows the important role that this region plays in the composite behaviour for relatively low indentation depths, as stated in [6].

*Corresponding author. Tel.: +351 239790700.
E-mail address: nataliya.sakharova@dem.uc.pt (N.A. Sakharova).

0272-8842/$ - see front matter © 2013 Elsevier Ltd and Techna Group S.r.l. All rights reserved.
http://dx.doi.org/10.1016/j.ceramint.2013.01.046

The experimental procedure associated with the use of depth-sensing indentation tests requires a careful preparation of the sample surface. This is particularly important, when using very low indentation depths, which reduce the accuracy of the evaluated mechanical properties. In fact, uncertainties in the depth-sensing indentation data due to the roughness of the sample surface and the indenter's geometrical imperfections are inevitable, to a certain extent (see, for example, [7–9]).

Therefore, alternative methods have been proposed for determining the film's hardness considering the effect of the substrate on the film mechanical properties. The typical approach for solving this problem consists of performing hardness tests at relatively high indentation depths, then separating the contributions of the film and the substrate in the composite response. In a number of experimental and theoretical studies, different phenomenological and empirical weight functions for extracting the film hardness from the composite indentation data have been proposed, e.g. [10,11]. These functions are expressed by the general formulation:

$$\frac{H_C - H_S}{H_F - H_S} = \alpha(h_c/t), \tag{1}$$

where $\alpha(h_c/t)$ is a function of the ratio h_c/t (or its inverse t/h_c).

In some models, the $\alpha(h_c/t)$ function contains parameters with fixed values, in such a way that a unique equation can be used, whatever the film and substrate mechanical properties. For example, in case of the well-known Jönsson and Hogmark model [10], this function is:

$$\alpha = 2D\left(\frac{t}{d}\right) - D^2\left(\frac{t}{d}\right)^2, \tag{2}$$

where d is the diagonal of the Vickers indentation ($d = 7h_c$) and D is a predetermined parameter ($D \approx 1$ if, during indentation, only plastic strain occurs; and $D \approx 0.5$ if cracking also occurs in the coating). For applying this type of model, it is only necessary to perform a single hardness measurement on the composite, for a given h_c/t ratio, which is an advantage.

However, experimental results clearly show that the behaviour described by the $\alpha(h_c/t)$ function is not unique, but depends on the film and substrate mechanical properties and, possibly, on the indentation size effect of both materials (see for example [6,12,13]). In fact, experimental plots of $(H_C - H_S)/(H_F - H_S)$ *versus* h_c/t (or t/h_c) pointed out that enormous differences in this behaviour can be observed, see for example [1,11].

A few $\alpha(h_c/t)$ functions have been proposed to be fitted to the experimental evolution of the composite hardness results *versus* the relative contact indentation depth, h_c/t; the parameters of these functions depend on the properties of the composite material. For example, in the case of the Korsunsky model [14]:

$$\frac{H_C - H_S}{H_F - H_S} = \frac{1}{1 + k(h_c/t)^2}, \tag{3}$$

where k is a dimensionless parameter, given by the ratio: $k = t/\gamma$; in which γ, that has the dimension of length, is linked to the fracture toughness. For the fracture-dominated case (when facture occurs) γ is proportional to the film thickness, t; while for the plastically-dominated case (when fracture does not occur), γ mainly depends on the ratio H_F/H_S and is weakly dependent on t. The quality of the fit used in this model depends on the experimental hardness data obtained over a wide range of h_c/t values, which implies that nanoindentation data are taken in account. Otherwise, there are insufficient data points for values close to zero to provide a good quality of the fit. Therefore, the main difficulty associated with this type of models is obtaining the correct extrapolation for h_c/t equal to zero.

In the literature, experimental results show three different regions in the plot of $(H_C - H_S)/(H_F - H_S)$ (or H_C) as a function of t/h_c (or h_c^{-1}, for a given film thickness of the composite) (see for example [1,15]). In one of these regions, which corresponds to relatively low indentation depths (i.e. high values of t/h_c), the evolution tends to gradually saturate ($(H_C - H_S)/(H_F - H_S) \to 1$). In the opposite region, for relatively high indentation depths (low values of t/h_c), the value of $(H_C - H_S)/(H_F - H_S)$ remains close to zero, from the origin of the axes up to a t/h_c value, depending on the composite, after which it shows a positive concavity. Finally, a relatively large region between the two previous regions with a linear evolution of $(H_C - H_S)/(H_F - H_S)$ *versus* t/h_c is observed, (see for example [13,16,17]).

In this context, we report a three-dimensional numerical simulation of the Vickers hardness test of several composites in order to study the linear region of the function $(H_C - H_S)/(H_F - H_S)$ *versus* t/h_c. Based on the numerical simulation results, a methodology for evaluation of the film hardness is developed. This approach consists of a simple method, which considers the hardness behaviour of the composite described by a linear $\alpha(h_c/t)$ function, with parameters that depend on the film/substrate system, and which avoids the use of indentation data obtained for very low indentation depths. The proposed methodology is validated using numerical and experimental indentation results.

2. Theoretical aspects

Depth-sensing indentation is commonly used for determining materials' hardness and Young's modulus. The hardness, H_{IT}, is evaluated by:

$$H_{IT} = \frac{P}{A}, \tag{4}$$

where P is the maximum load and A is the indentation contact area at maximum load.

The mechanical property results strongly depend on the accuracy of the value of the indentation contact area. In the case of Vickers or Berkovich ideal indenters, the contact area,

A, is given by:

$$A = 24.5\, h_c^2, \tag{5}$$

where h_c is the indentation contact depth, determined from the load–unloading curve using the equation [18]:

$$h_c = h_{max} - \varepsilon PC, \tag{6}$$

in which h_{max} is the indentation depth at maximum load, C the compliance of the unloading curve and ε an indenter geometrical parameter, which for the Vickers indenter is equal to 0.75. The compliance, C, can be evaluated by fitting the unloading curve, using the power law [8]:

$$P = P_0 + T(h - h_0)^m, \tag{7}$$

where T and m are constants obtained in the fit and h_0 is the indentation depth, which corresponds to a load value of P_0, during unloading. In the present study, Eq. (7) was fitted to 70% of the unloading curve [8].

3. Numerical simulation and materials

Three-dimensional numerical simulations of the Vickers hardness test were performed using the DD3IMP in-house code, which was developed to simulate processes involving large plastic deformations and rotations [19,20]. This code considers the hardness test as a quasi-static process and makes use of a fully implicit algorithm of Newton-Rapson type to solve the strong non-linearities related to the large deformations and rotations, the elastoplastic mechanical behaviour and the contact with friction conditions. The DD3IMP code allows simulating the hardness test with any type of indenter geometry, taking into account the contact with friction between the indenter and the sample. In the present study, the friction was assumed to be described by a Coulomb coefficient equal to 0.16 [8].

The Vickers indenter geometry was modelled using parametric Bézier surfaces, which enable a fine description of the indenter tip, namely the offset geometrical imperfection, which occurs in the real geometry [8,9,21]. In this

Table 1
Mechanical properties of the composites (Fi=F1 to F6, films and Si=S1 to S30, substrates) used in the numerical simulations.

	Material	σ_y (GPa)	n	v	E (GPa)	H (GPa)	H_F/H_S		E_F/E_S	
Group 1	F1	*5.50*	*0.01*	*0.22*	*500*	*17.98*	F1/Si	F2/Si	F1/Si	F2/Si
	F2	*5.50*	*0.01*	*0.29*	*220*	*14.96*				
	S1	0.25	0.01	0.29	220	1.13	15.96	13.28	2.27	1.00
	S2	0.32	0.01	0.29	220	1.42	12.72	10.58		
	S3	0.22	0.30	0.33	140	1.65	10.89	9.06	3.57	1.57
	S4	0.47	0.01	0.29	220	2.01	8.94	7.44	2.27	1.00
	S5	0.59	0.01	0.29	220	2.55	7.02	5.84		
	S6	0.63	0.16	0.29	220	3.35	5.38	4.48		
	S7	0.87	0.04	0.29	220	3.62	4.96	4.13		
	S8	1.05	0.04	0.29	220	4.22	4.27	3.55		
	S9	1.45	0.04	0.29	220	5.54	3.25	2.70		
	S10	2.63	0.01	0.29	220	8.70	2.07	1.72		
Group 2	F3	*2.48*	*0.01*	*0.22*	*500*	*9.16*	F3/Si	F4/Si	F3/Si	F4/Si
	F4	*2.48*	*0.01*	*0.29*	*220*	*8.35*				
	S11	0.14	0.01	0.29	220	0.67	13.77	12.56	2.27	1.00
	S12	0.18	0.01	0.29	220	0.82	11.20	10.22		
	S13	0.12	0.30	0.33	140	0.99	9.27	8.46	3.57	1.57
	S14	0.26	0.01	0.29	220	1.15	7.98	7.27	2.27	1.00
	S15	0.33	0.01	0.29	220	1.45	6.35	5.79		
	S16	0.34	0.16	0.29	220	1.93	4.72	4.31		
	S17	0.52	0.04	0.29	220	2.35	3.89	3.55		
	S18	0.55	0.04	0.29	220	2.50	3.67	3.34		
	S19	0.70	0.04	0.29	220	3.06	3.00	2.74		
	S20	1.26	0.01	0.29	220	4.65	1.97	1.80		
Group 3	F5	*5.50*	*0.01*	*0.22*	*300*	*15.20*	F5/Si	F6/Si	F5/Si	F6/Si
	F6	*5.50*	*0.01*	*0.29*	*132*	*12.92*				
	S21	0.26	0.01	0.29	132	1.09	14.01	11.90	2.27	1.00
	S22	0.33	0.01	0.29	132	1.38	11.05	9.38		
	S23	0.22	0.30	0.33	84	1.59	9.57	8.13	3.57	1.57
	S24	0.47	0.01	0.29	132	1.94	7.86	6.68	2.27	1.00
	S25	0.59	0.01	0.29	132	2.28	6.64	5.64		
	S26	0.63	0.16	0.29	132	3.18	4.76	4.04		
	S27	0.87	0.04	0.29	132	3.34	4.56	3.87		
	S28	1.05	0.04	0.29	132	3.93	3.87	3.29		
	S29	1.45	0.04	0.29	132	5.12	2.96	2.52		
	S30	2.63	0.01	0.29	132	7.45	2.04	1.73		

study, the Vickers indenter has a tip imperfection, which consists of a plane normal to the indenters' axis with an area equal to 0.0032 μm^2.

The sample used in numerical simulations of the hardness tests has a cylindrical geometry, where the radius and height are both equal to 40 μm. Different film thicknesses were considered (t = 0.03, 0.06, 0.12, 0.30, 0.42, 0.60, 0.75, 1.05, 1.20, 1.35, 1.65, 2.00, 2.40 μm) in order to obtain several relative indentation contact depths, using a fixed value of the maximum indentation depth equal to 0.3 μm. The mesh discretisation was performed using three-linear eight-node isoparametric hexahedrons. Due to the sample's cylindrical symmetry, only one quarter of the sample was used in the numerical simulation of the Vickers hardness test. The mesh refinement was chosen in order to provide accurate values of the indentation contact area and, consequently, of the mechanical properties [8].

The elastic behaviour is considered isotropic and is defined by Young's modulus, E, and Poisson coefficient, ν. Table 1 summarises the mechanical properties of the films and the substrate materials studied. The numerical simulations of the Vickers hardness tests were performed on three groups of twenty composites. In each group, ten different substrates coated with two distinct film materials were considered. Overall, more than seven hundred numerical simulations on composites with different ratios between the film, H_F, and substrate, H_S hardnesses (ten different cases of substrate for each film, with ratios H_F/H_S between 1.72 and 15.91) as well as between the film, E_F, and substrate, E_S, Young's modulus (ratios: E_F/E_S equal to 1.00 and 2.27) were studied. Note that for the composites with the substrates S3, S13 and S23 (one from each group in Table 1), the Young's modulus ratio (E_F/E_S equal to 1.57 and 3.57) is different from the other cases in the same set. The purpose of including them was to obtain specific data points concerning trends analysed in the study.

The plastic behaviour of the materials used in the numerical simulations was modelled considering that the stress, σ, and plastic strain, ε, relationship was described by the Swift law (see for example [22]: $\sigma = K(\varepsilon+\varepsilon_0)^n$, where K, ε_0 and n (work-hardening coefficient) are material constants (the material yield stress is: $\sigma_y = K\varepsilon_0^n$). The constant ε_0 was considered to be equal to 0.005 for all materials.

4. Results and discussion

4.1. Composite hardness

Fig. 1 shows examples of the evolution of the composite hardness, H_C, as a function of indentation contact depth normalised by the film thickness, h_c/t, for the case of films F1 and F3 on the substrates S1 to S10 and S11 to S20, respectively. These examples reveal that, for values of h_c/t lower than about 1, the composite hardness quickly approaches the film hardness, with decreasing h_c/t. It is possible to identify three regions of substrate influence on composite hardness. For high values of h_c/t, the measured

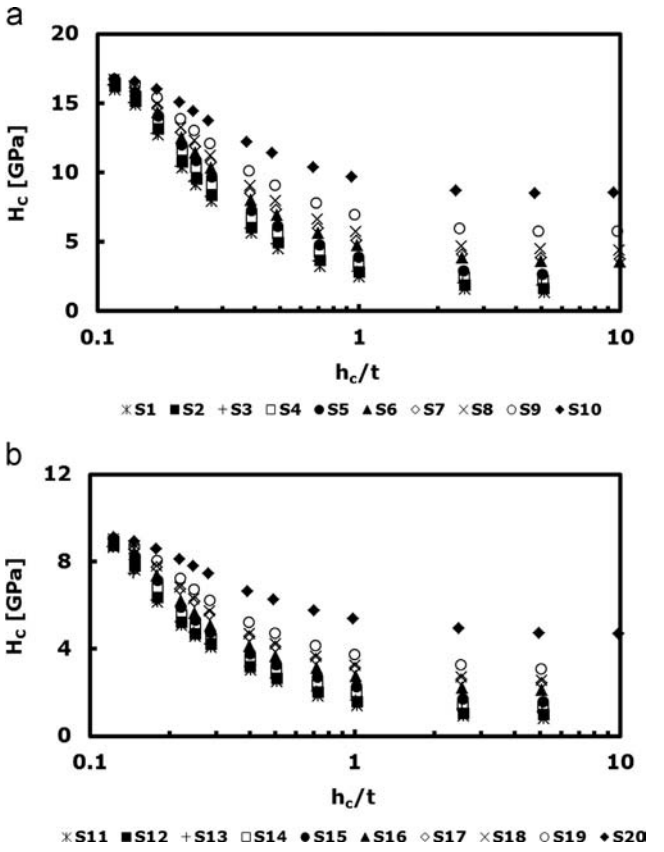

Fig. 1. Hardness of composites, *Hc*, *versus* the contact indentation depth normalised by the film thickness, h_c/t for (a) film F1 on soft substrates S1–S10 and (b) film F3 on soft substrates S11–S20.

hardness is similar to that of the substrate. For intermediate h_c/t values, the hardness of the film/substrate system is strongly influenced by the value of h_c/t. In the case of small values of the ratio h_c/t (close to 0.1, but depending on the ratio H_F/H_S), the substrate almost does not contribute to the measured hardness, and so H_C is close to the film hardness, H_F.

For further understanding of the composite hardness behaviour, the above results were analysed by plotting $(H_C-H_S)/(H_F-H_S)$ as a function of t/h_c. These results are shown in Fig. 2 for the same film/substrate systems as in Fig. 1. Three different stages can also be identified in these plots, as exemplified in Fig. 2(a). Similar trends, emphasising these three different stages of composite hardness behaviour, have been experimentally observed, such as in the cases of thick (155–440 μm) Cr_3C_2/NiCr coatings on low carbon steel in [23] and W–C–Co coatings on copper and mild steel substrates [1]. In stage I, for small values of t/h_c ($t/h_c < 1$), the ratio $(H_C-H_S)/(H_F-H_S)$ approaches zero, in a nonlinear fashion. Fig. 2(a) shows a detail of this region. Such behaviour is due to the insignificant influence of the film on the hardness of the film/substrate system, throughout stage I (high values of h_c/t). During stage II, for t/h_c values in the range of 1–6, the composite behaviour can be approximately represented by a

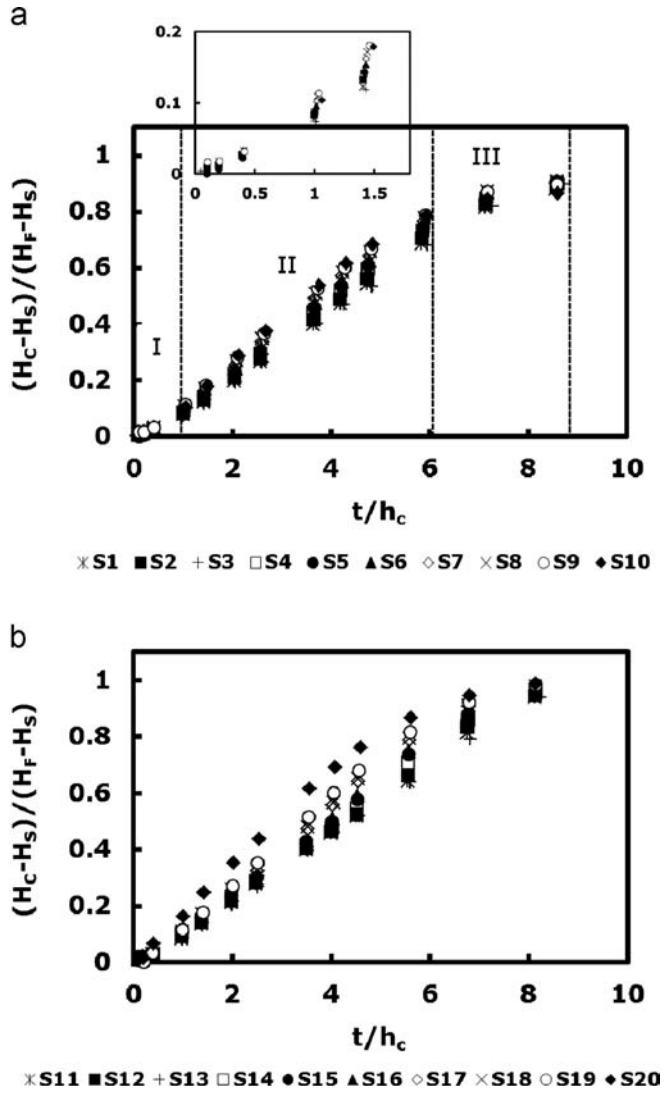

Fig. 2. Ratio $(H_C-H_S)/(H_F-H_S)$ as a function of t/h_c: (a) film F1 on substrates S1–S10, identifying the three stages: I, II and III and (b) film F3 on substrates S11–S20.

straight line, with a slope that depends on the substrate and film mechanical properties: the smaller the ratio H_F/H_S, the higher the slope of the linear relation, as shown in Fig. 3. This behaviour agrees with previously reported results [1,19,23,24]. For values of t/h_c higher than about 6, stage III (Fig. 2(a)), the ratio $(H_C-H_S)/(H_F-H_S)$ slowly approaches 1. This is a consequence of the decrease in the substrate effect on composite hardness. In general, the measured hardness of the composite, H_C, is very close to the film hardness, H_F, for t/h_c values close to 9.

In order to understand the composite hardness behaviour, during the course of the three stages highlighted above, the equivalent plastic strain distribution in the composites was studied. Fig. 4 shows examples of the equivalent plastic strain distribution obtained for the composite F1/S10, at different values of the ratio t/h_c (6.35, 2.55 and 0.43) chosen in order to cover all three stages of the plot $(H_C-H_S)/(H_F-H_S)$ *versus* t/h_c. With

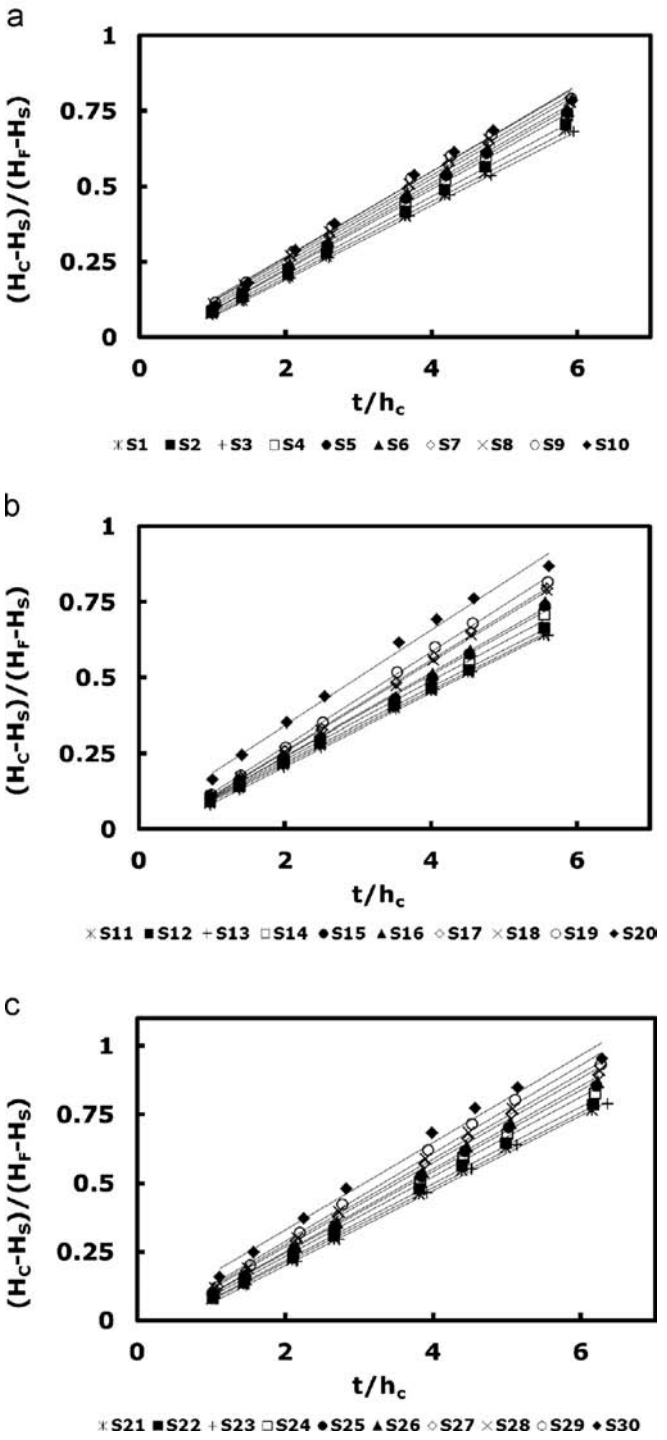

Fig. 3. Ratio $(H_C-H_S)/(H_F-H_S)$ as a function of t/h_c: (a) film F1 on substrates S1–S10; (b) film F3 on substrates S11–S20 and (c) film F5 on substrates S21–S30.

the decrease of the ratio t/h_c, i.e. the increase of the relative indentation depth, h_c/t, the plastic strain distribution progresses from the film into the substrate. In the case of Fig. 4(a), the region with plastic strain is located only in the film, and the substrate does not show plastic strain, indicating that the test was conducted during stage III.

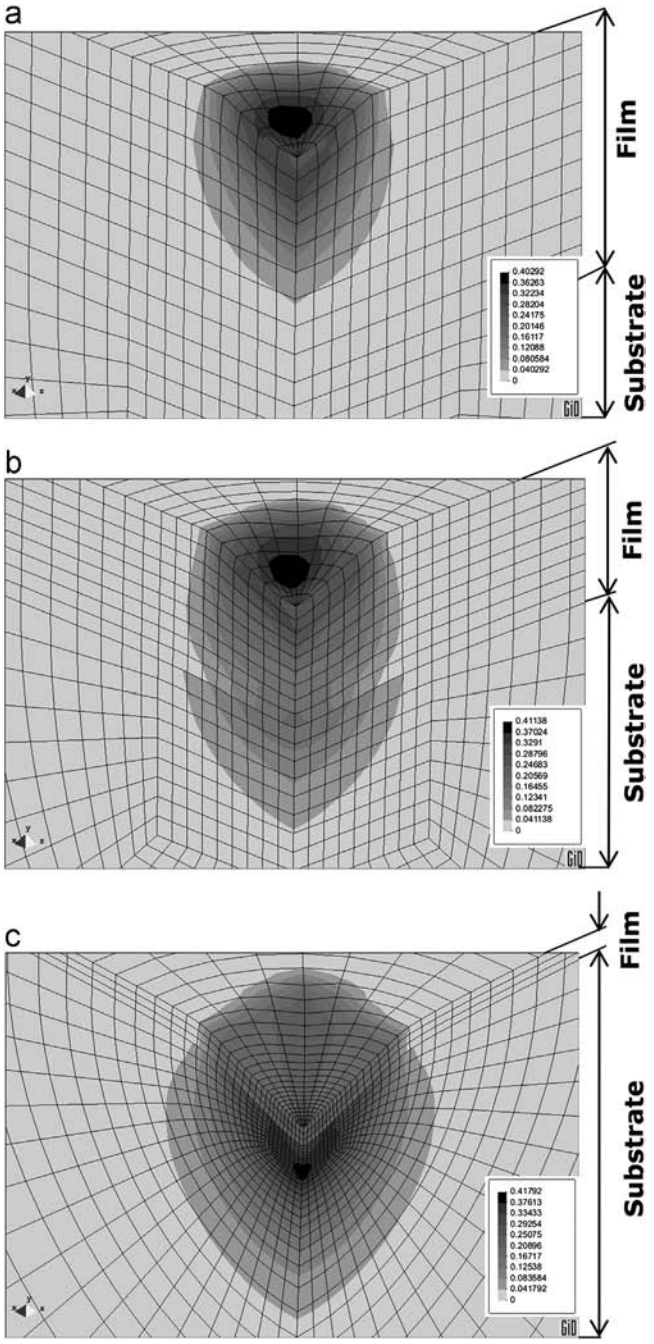

Fig. 4. Equivalent plastic strain distribution for F1/S10 film/substrate system: (a) $t/h_c=6.35$, stage III; (b) $t/h_c=2.55$, stage II and (c) $t/h_c=0.43$, stage I.

Since the substrate does not contribute to the overall plastic deformation of the film/substrate system, the composite hardness, H_C, is not significantly affected by the substrate hardness, H_S (only elastic deformation occurs in the substrate). As the relative indentation depth increases, stage II begins and the feature of the equivalent plastic strain distribution changes (Fig. 4(b)). The plastically deformed region enlarges and becomes deeper, reaching the substrate. However, both the maximum value of the equivalent plastic strain and its location in the film (close to the indenter tip) remain identical to those of Fig. 4(a) (close to the end of the stage III). Therefore, the most distinctive feature between stages III and II is the fact that plastic deformation occurs in the substrate during the latter. In fact, with the increase of the relative indentation depth during stage II, the size of the plastically deformed region and the maximum value of the equivalent plastic strain increase in the substrate.

A further increase of the indentation depth causes the transition to stage I. During this stage, the values of the equivalent plastic strain in the film—the maximum value and those in the nearby regions—remain at the same level as during stage II, although the deformed region is extended parallel to the surface of the sample. In the substrate, the deformed region enlarges and the maximum value of equivalent plastic strain increases, as stage I progresses (Fig. 4(c)). Similar plastic strain distributions were obtained for the other composites, shown in Table 1.

Fig. 5(a,b) summarises the main features of the maximum plastic strain evolutions in the film during stages I, II

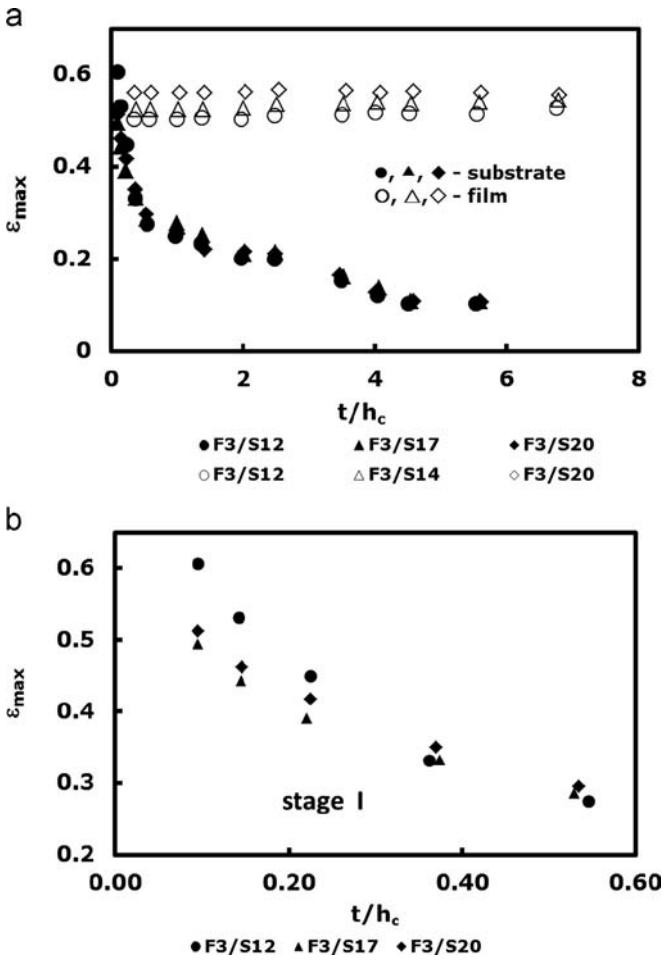

Fig. 5. Evolution of the maximum equivalent strain value *versus* t/h_c (a) for the film during the stages I, II and III, and for the substrate during the stages I and II for film/substrate systems F3/S12, F3/S17 and F3/S20; (b) detailed view for the substrate during the stages I.

and III, and in the substrate during stages I and II, using the examples of the composites F3/S12, F3/S17 and F3/S20. It is seen that the maximum value of the equivalent plastic strain in the film quickly reaches a stable value, even during stage III (at the beginning of the test), which is maintained throughout the remaining stages of the plot $(H_C-H_S)/(H_F-H_S)$ *versus* t/h_c. The maximum value of the equivalent plastic strain in the substrate increases with

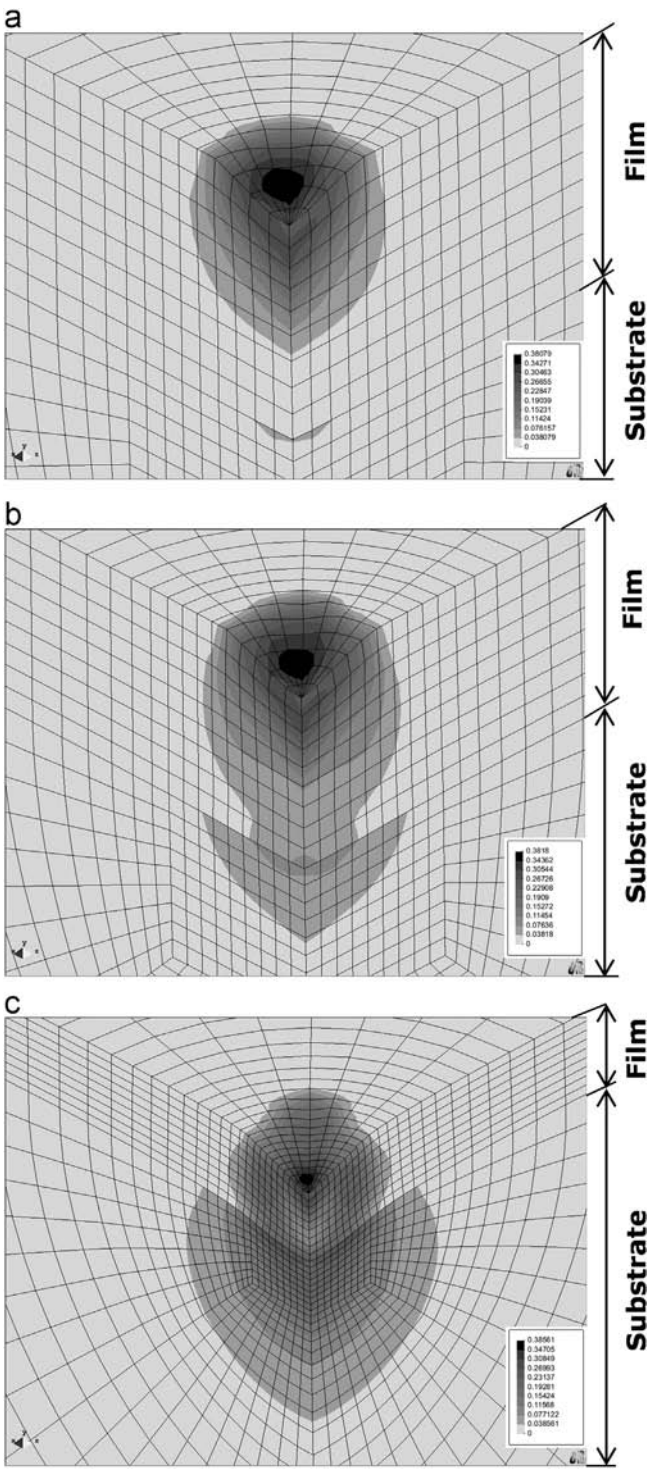

Fig. 6. Equivalent strain distribution during an indentation test in F1/S2 film/substrate system with $H_F/H_S = 12.72$ for the case of $t=0.6$ μm at indentation depth: (a) $h=0.100$ μm; (b) $h=0.127$ μm and (c) $h=0.313$ μm.

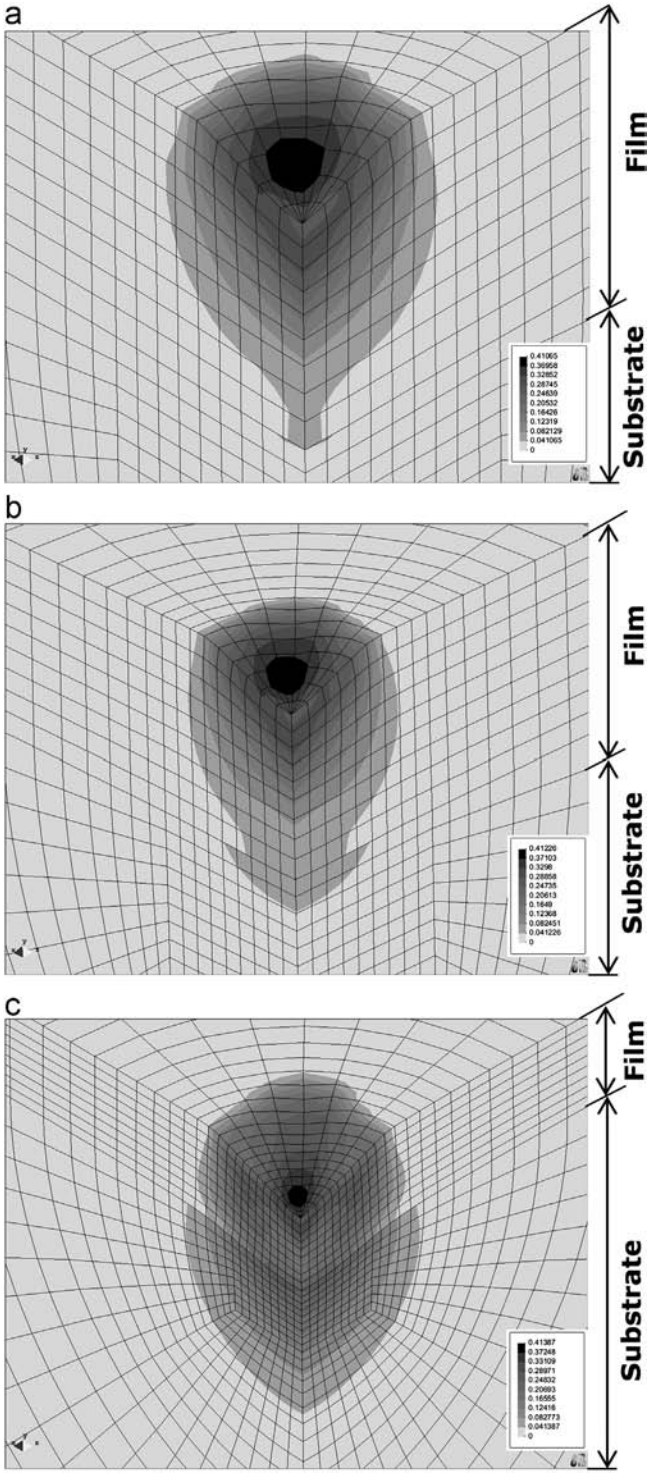

Fig. 7. Equivalent strain distribution during an indentation test in F1/S10 system with $H_F/H_S=2.07$ for the case of $t=0.6$ μm at indentation depth: (a) $h=0.110$ μm; (b) $h=0.138$ μm and (c) $h=0.313$ μm.

the decrease of the ratio t/h_c; this trend is very pronounced for stage I (at the end of the indentation test, *i.e.* for low values of t/h_c). Moreover, in the case of the substrate with a lower value of yield stress (higher value of the ratio H_F/H_S), *i.e.* for the composite F3/S12, the maximum value of the plastic strain attained during stage I is higher than for the cases of the composites F3/S17 and F3/S20, as seen in the detailed part of the graph on Fig. 5(b). In this context, the character of the equivalent plastic strain distribution during stage I confirms that, during this phase, the substrate contributes considerably towards the composite hardness.

Fig. 6 shows the evolution of the equivalent plastic strain distribution as a function of the indentation depth, obtained during a test with the composite F1/S2 ($H_F/H_S = 12.72$), with a film thickness equal to 0.60 μm. The substrate, with relatively low hardness, starts deforming, plastically, adjacent to the interface with the substrate (plastic deformation of the film is already visible in Fig. 6(a)), when the deformed region of the film is still relatively small. Then, the region with plastic strain grows within the substrate and becomes wider than that within the film (Fig. 6(b) and (c)). Fig. 7 presents the same distributions obtained in the case of a relatively harder substrate, the F1/S10 system with $H_F/H_S = 2.07$ and a film thickness equal to 0.60 μm. In this case, the substrate only begins to deform plastically after the film region, contiguous to the substrate, has already been plastically deformed (Fig. 7(a)). Subsequent growing of the plastically deformed region within the substrate does not lead to any significant enlargement (Fig. 7(b) and (c)), compared with the previous case of the relatively very soft substrate. Therefore, at a given indentation depth, the relative size of the plastically deformed region in the substrate depends on the ratio H_F/H_S, and decreases when this ratio decreases (compare Fig. 6(c) and Fig. 7(c), for example). In the context above, it can be concluded that the feature of the equivalent plastic strain distribution in the substrate influences the mechanical behaviour of the composite, in particular during stage II, namely the slope of the straight lines of the plot $(H_C-H_S)/(H_F-H_S)$ *versus* t/h_c, which depends on the mechanical properties of the film and the substrate.

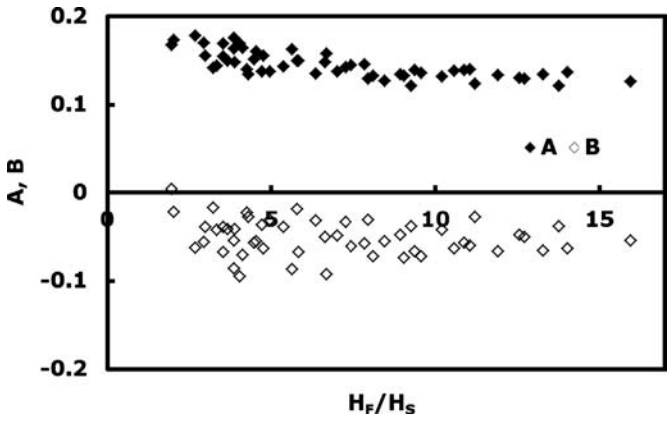

Fig. 8. Parameters A and B *versus* H_F/H_S for all considered film/substrate systems.

4.2. Film hardness determination

Based on the behaviour described above, particularly in the linear relation observed between $(H_C-H_S)/(H_F-H_S)$ *versus* t/h_c during stage II, also previously observed experimentally (see for example: [1,13,16,17]), a simple model for determining the film hardness for a film/substrate system is developed.

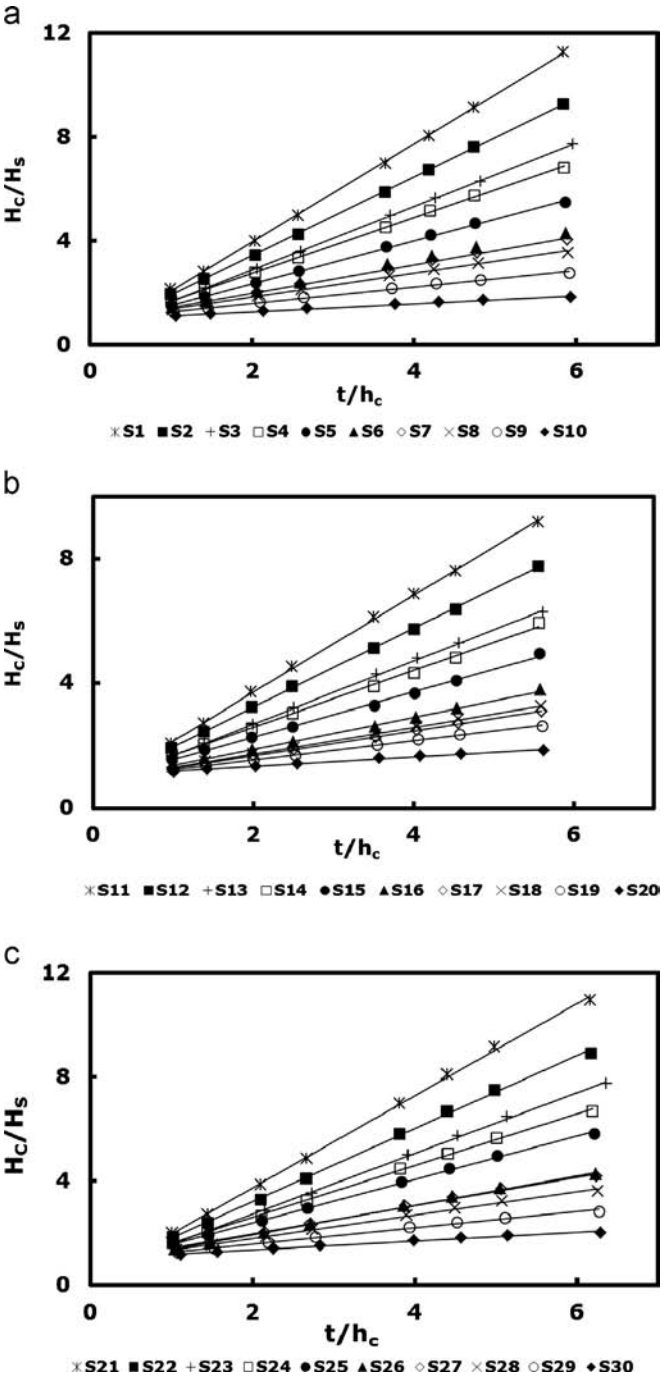

Fig. 9. Linear fitting of the numerical data during stage II. Ratio H_C/H_S as a function of t/h_c: (a) film F1 on substrates S1–S10; (b) film F3 on substrates S11–S20 and (c) film F5 on substrates S21–S30.

The linearity observed during stage II is described by an equation of the type:

$$\frac{H_C - H_S}{H_F - H_S} = A\left(\frac{t}{h_c}\right) + B, \quad (9)$$

where A and B are parameters that can be obtained by fitting Eq. (9) to the composite hardness data obtained at different values of the ratio t/h_c. The parameter A characterises the slope of the straight lines from the plot $(H_C - H_S)/(H_F - H_S)$ as a function of t/h_c. Fig. 8 shows the evolution of the parameters A and B, as a function of the ratio H_F/H_S, obtained for all the tested composites. Parameter A decreases slightly with an increase of the ratio H_F/H_S. This trend and the current values of the parameter A are in reasonable agreement with those previously observed experimentally [1].

From Eq. (9), the ratio H_C/H_S can be written as follows:

$$\frac{H_C}{H_S} = k_1\left(\frac{t}{h_c}\right) + k_2 \quad (10)$$

where k_1 and k_2 are parameters given by:

$$k_1 = \left(\frac{H_F}{H_S} - 1\right)A \quad (11)$$

Table 2
Values of k_1 obtained in the linear fitting of the numerical data H_C/H_S as a function of t/h_c (Eq. (10)).

Substrate		k_1	H_F/H_S		k_1	H_F/H_S
S1	Film F1	2.126	15.96	Film F2	1.646	13.28
S2		1.514	12.72		1.322	10.58
S3		1.219	10.89		1.073	9.06
S4		1.070	8.94		0.930	7.44
S5		0.828	7.02		0.742	5.84
S6		0.601	5.38		0.526	4.48
S7		0.551	4.96		0.491	4.13
S8		0.456	4.27		0.409	3.55
S9		0.317	3.25		0.281	2.70
S10		0.153	2.07		0.127	1.72
S11	Film F3	1.551	13.77	Film F4	1.486	12.56
S12		1.262	11.20		1.200	10.22
S13		1.006	9.27		0.948	8.46
S14		0.905	7.98		0.829	7.27
S15		0.721	6.35		0.630	5.79
S16		0.512	4.72		0.445	4.31
S17		0.428	3.89		0.363	3.55
S18		0.400	3.67		0.339	3.34
S19		0.311	3.00		0.259	2.74
S20		0.153	1.97		0.124	1.80
S21	Film F5	1.776	14.01	Film F6	1.458	11.90
S22		1.406	11.05		1.166	9.38
S23		1.168	9.57		0.944	8.13
S24		0.997	7.86		0.838	6.68
S25		0.837	6.64		0.700	5.64
S26		0.568	4.76		0.474	4.04
S27		0.548	4.56		0.458	3.87
S28		0.449	3.87		0.372	3.29
S29		0.315	2.96		0.251	2.52
S30		0.166	2.04		0.117	1.73

$$k_2 = 1 + \left(\frac{H_F}{H_S} - 1\right)B \quad (12)$$

Fig. 9 shows the evolution of the ratio H_C/H_S as a function of t/h_c (Eq. 10), in the case of films F1, F3 and F5 and all the substrates of groups 1, 2 and 3, for values of the ratio t/h_c in the range between 1.0 and 6.0, *i.e.* during stage II. The evolutions obtained can be described by straight lines, with slope, k_1 (see Eq. (10)), that increases with the ratio H_F/H_S. Similar results were obtained for all the composites studied. Table 2 summarises the values of k_1 obtained for all values of the ratio H_F/H_S.

The evolution of the ratio H_F/H_S as a function of k_1 is nearly linear. Fig. 10(a) shows this evolution for all film/substrate systems studied. Therefore, k_1 can be considered as a measurement of the relative film hardness (*i.e.* of the H_F/H_S ratio). The evolutions in Fig. 10(a), can be expressed by a simple linear equation deduced from Eq. (11), such as:

$$\frac{H_F}{H_S} = ak_1 + 1 \quad (13)$$

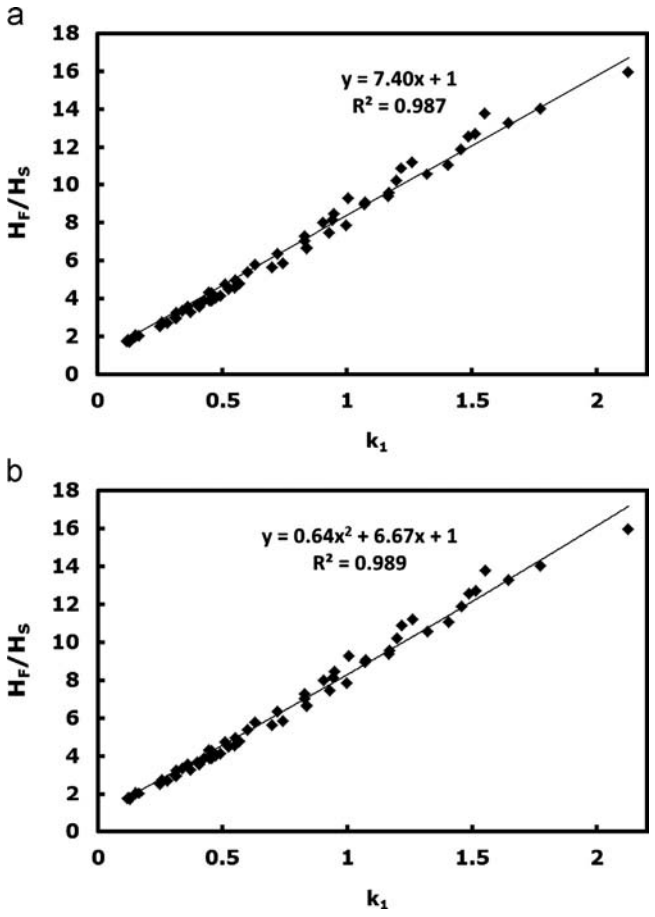

Fig. 10. Linear (a) and second order polynomial (b) fitting of the numerical data during stage II: ratio H_F/H_S *versus* k_1 for all composites studied.

Table 3
Results of the film hardness obtained for the fictitious composites in Table 1, using the proposed methodology.

Composite	Reference value $H_{F,}$ GPa	Eq. (14)	error (%)	Eq. (15)	error %
F1/S1	17.98	18.85	4.8	20.35	13.2
F1/S2		17.26	−4.0	17.77	−1.2
F1/S3		16.54	−8.0	16.64	−7.5
F1/S4		17.93	−0.3	17.83	−0.8
F1/S5		18.26	1.6	17.84	−0.8
F1/S6		18.21	1.3	17.51	−2.6
F1/S7		18.41	2.4	17.66	−1.8
F1/S8		18.44	2.6	17.60	−2.1
F1/S9		18.53	3.1	17.61	−2.1
F1/S10		18.54	3.1	17.70	−1.6
F2/S1	14.96	14.85	−0.7	15.44	3.2
F2/S2		15.25	1.9	15.46	3.3
F2/S3		14.76	−1.3	14.69	−1.8
F2/S4		15.85	5.9	15.60	4.3
F2/S5		16.64	11.2	16.15	8.0
F2/S6		16.36	9.4	15.66	4.7
F2/S7		16.80	12.3	16.06	7.4
F2/S8		16.98	13.5	16.17	8.1
F2/S9		17.06	14.0	16.21	8.4
F2/S10		16.87	12.8	16.16	8.0
F3/S11	9.16	8.30	−9.4	8.57	−6.4
F3/S12		8.45	−7.8	8.53	−6.9
F3/S13		8.34	−9.0	8.25	−9.9
F3/S14		8.84	−3.5	8.68	−5.2
F3/S15		9.14	−0.2	8.86	−3.3
F3/S16		9.29	1.4	8.89	−2.9
F3/S17		9.82	7.2	9.36	2.2
F3/S18		9.89	8.0	9.42	2.8
F3/S19		10.08	10.0	9.58	4.6
F3/S20		9.91	8.2	9.46	3.3
F4/S11	8.35	7.98	−4.4	8.20	−1.8
F4/S12		8.07	−3.4	8.11	−2.9
F4/S13		7.91	−5.3	7.80	−6.6
F4/S14		8.19	−1.9	8.00	−4.2
F4/S15		8.17	−2.2	7.87	−5.7
F4/S16		8.32	−0.4	7.94	−4.9
F4/S17		8.68	4.0	8.26	−1.1
F4/S18		8.76	4.9	8.33	−0.2
F4/S19		8.90	6.6	8.46	1.3
F4/S20		8.91	6.7	8.53	2.2
F5/S21	15.20	15.34	0.9	16.12	6.1
F5/S22		15.69	3.2	16.01	5.3
F5/S23		15.32	0.8	15.35	1.0
F5/S24		16.20	6.6	16.02	5.4
F5/S25		16.47	8.4	16.09	5.9
F5/S26		16.62	9.3	15.95	4.9
F5/S27		16.87	11.0	16.17	6.4
F5/S28		16.97	11.6	16.19	6.5
F5/S29		17.10	12.5	16.24	6.8
F5/S30		16.59	9.1	15.82	4.1
F6/S21	12.92	12.80	−0.9	13.12	1.5
F6/S22		13.26	2.6	13.28	2.8
F6/S23		12.70	−1.7	12.51	−3.2
F6/S24		13.93	7.8	13.62	5.4
F6/S25		14.16	9.6	13.70	6.0
F6/S26		14.41	11.5	13.76	6.5
F6/S27		14.66	13.5	13.99	8.3
F6/S28		14.75	14.2	14.03	8.6
F6/S29		14.68	13.6	13.94	7.9
F6/S30		13.90	7.6	13.33	3.2

where the coefficient a is the inverse of the A parameter: $a = 1/A$ (see Eq. (11)).

So, considering the value of coefficient a, obtained from Fig. 10(a) ($a = 7.40$) we can rewrite Eq. (13) as follows:

$$\frac{H_F}{H_S} = 7.40k_1 + 1 \quad (14)$$

In this context, it is possible to extract the relative film hardness, H_F/H_S, using Eq. (14), where the k_1 value can be determined from the experimental normalised composite hardness, H_C/H_S, obtained at different indentation depths (see examples in Fig. 9 of plots H_C/H_S *versus* t/h_c).

The description of the evolution of the ratio H_F/H_S as a linear function of k_1 is somewhat simplified due to the fact that the parameter A decreases slightly with the increase of the ratio H_F/H_S (see Fig. 8); consequently, the coefficient a, which is the inverse of the A parameter, also evolves with the ratio H_F/H_S and, therefore, depends on k_1. In order to describe the ratio H_F/H_S as a function of k_1 more accurately, the numerical results were also fitted using a second order polynomial, as shown in Fig. 10(b). This corresponds to expressing the a coefficient by a linear function of k_1: $a = C_1k_1 + C_2$, where C_1 and C_2 are linearity constants. Similarly to the procedure used in Eq. (14), it is possible to extract the relative value of the film's hardness, H_F/H_S, using the following equation:

$$\frac{H_F}{H_S} = 0.64k_1^2 + 6.67k_1 + 1 \quad (15)$$

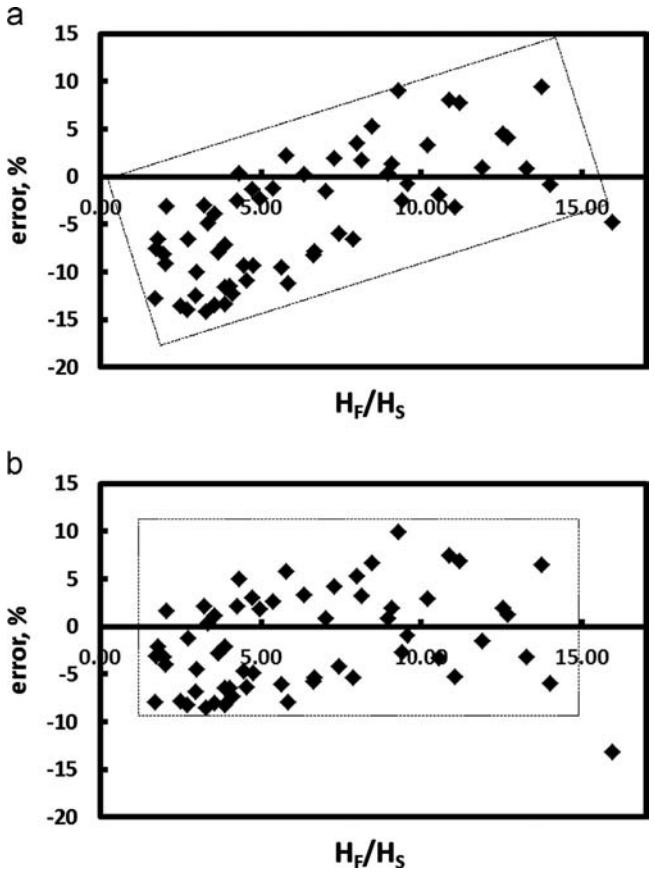

Fig. 11. Error in determining film hardness for the composites of Table 1, with recourse to: (a) linear equation, Eq. (14) and (b) second order polynomial equation, Eq. (15).

Table 4
Results of the film's hardness obtained from experimental data in literature, using the proposed methodology.

Ref.	Composite	Film hardness H_F, GPa	Substrate hardness H_S, GPa	Eq. (14)	error (%)	Eq. (15)	error (%)
[1]	WCCO/ACu	18.5	1.0	17.19	−7.1	18.65	0.8
	WCCO/RS		2.3	18.60	0.5	18.37	−0.7
	WCCO/M2A		3.5	19.17	3.6	18.44	−0.3
	WCCO/M2B		5.4	19.67	6.3	18.71	1.1
	WCCO/M2C		7.6	19.50	5.4	18.55	0.3
	WCCO/M2D		9.0	19.98	8.0	19.05	3.0
[5]	GaN/Sapphire	23.9	18.2	23.94	0.2	23.39	−2.1
	TiAlN/steel	19.0	2.1	18.90	−0.5	18.81	−1.0
	Fe-Ni-B/steel	11.0	1.3	11.05	0.5	10.94	−0.5
	TiCN/WC	40.0	19.8	40.00	0.0	38.24	−4.4
	Cr/brass	10.3	1.5	10.29	−0.1	10.02	−2.7
	Ni/Cu	5.5	1.4	5.70	3.6	5.43	−1.3
[25]	TiN/hss	23.5	17.0	25.74	9.5	24.93	6.1
[26]	Tungsten/Al	14.0	1.0	14.24	1.7	15.10	7.9
[27]	Al_2O_3/Al	10.0	1.5	10.02	0.2	9.74	−2.6
[28]	SiC/Si	30.5	18.0	30.83	1.1	29.67	−2.7
	TiN/steel	38.0	2.1	38.03	0.1	41.66	9.6
[29]	AlCrN/D2 tool steel	27.6	5.9	30.73	11.3	29.50	6.9
[30]	TiB_2/Si	35.0	18.0	35.30	0.9	33.79	−3.5
	TiB_2/stainless steel		3.5	38.22	9.2	38.81	10.9
[31]	TiB_2/glass	36.0	7.0	39.32	9.2	37.87	5.2
[32]	AlC/Si	7.0	5.0	7.56	8.0	7.33	4.7
	AlN/Si	10.5	5.0	11.09	5.6	10.57	0.7
	AlCN/Si	7.0	5.0	6.86	−2.0	6.69	−4.4
[33]	Al_2O_3/Al	22.0	1.4	21.22	−3.5	22.44	2.0

4.3. Model validation

The procedure proposed for the film hardness evaluation using Eq. (14) or (15), was tested using the fictitious composites of Table 1 and other composites taken from the literature. The results are shown in Tables 3 and 4, respectively and which enable us to conclude that accurate results are obtained for film hardness.

The error in the film hardness for fictitious composites from Table 1, evaluated with equation (Eq. (14)), is typically lower than 10% (only in a few cases of fictitious composites—11 of the 60 composites studied—the error reaches 11–14%), the average of the absolute values of the errors being equal to 6.2%. When assessing the film hardness of the same composites using the polynomial equation (Eq. (15)), the average of the absolute values of the errors decreases to 4.6%. In this case, the error does not normally exceed 10%, and only for one composite reaches 13.2%. Fig. 11(a) and (b) represent the errors of film hardness as a function of the ratio H_F/H_S, determined using the linear (Eq. (14)) and second order polynomial (Eq. (15)) equations, respectively. These figures show a balanced distribution of the positive and negative errors, along the H_F/H_S axis, in the case of using Eq. (15) (Fig. 11(b)), which does not occur when using Eq. (14) (Fig. 11(a)).

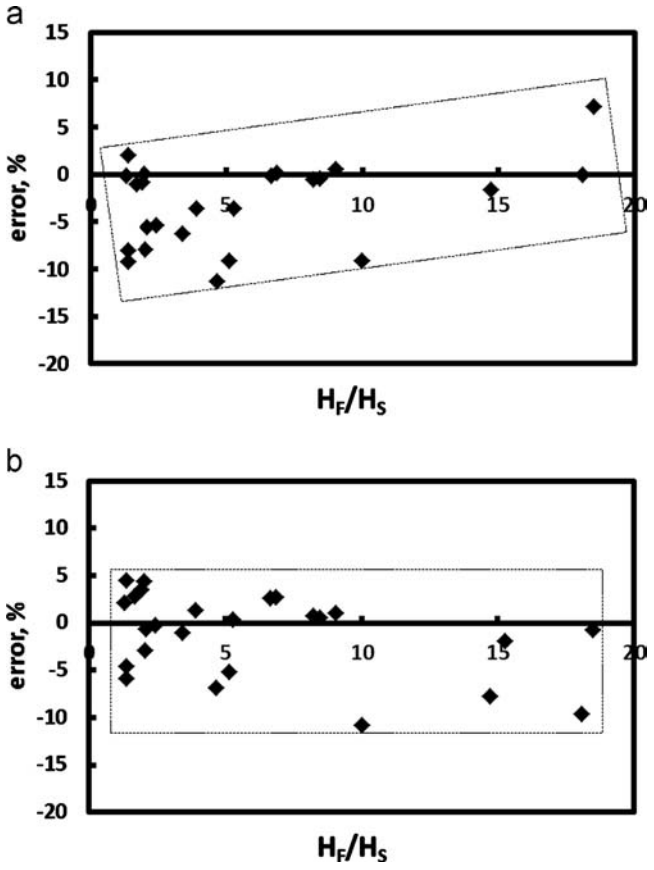

Fig. 12. Error in the determination of film hardness for composites taken from literature with recourse to: (a) linear equation, Eq. (14) and (b) second order polynomial equation, Eq. (15).

The error in the determination of the film hardness, in the case of the real composite materials taken from the literature, is lower than for the case of the fictitious composite studied here by numerical simulation. Table 4 shows that the average of the absolute values of the error in film hardness assessed using Eq. (14) is 3.9%, decreasing to 3.4% with Eq. (15). Moreover, as shown in Fig. 12(a) and (b), and as for the fictitious materials, the error distribution along the H_F/H_S axis using Eq. (15) is better balanced than with Eq. (14).

5. Conclusions

Based on numerical simulation results, a new methodology to determine the film hardness in film/substrate composites, using depth-sensing indentation data, has been proposed. The most common case, i.e. when the film is harder than the substrate, was considered. The application of the proposed methodology to several fictitious and real composites shows that accurate results for the film hardness can be obtained for a wide variety of composites.

The most relevant conclusions reached in this study can be summarised as follows:

During the indentation test of thin films on substrates, the plot $(H_C-H_S)/(H_F-H_S)$ *versus* t/h_c shows the presence of three stages. At the beginning of the test (stage III), the region with plastic deformation is located only in the film, and the substrate does not present plastic strain. As the relative indentation depth increases, the plastically deformed region in the film enlarges and becomes deeper, thus reaching the substrate (linear stage II starts). However, the maximum value of the equivalent plastic strain and its location in the film remains identical to that obtained closer to the end of stage III, when plastic deformation occurs in the substrate. With the increase of the relative indentation depth during stage II, the size of the plastically deformed region and the maximum value of the equivalent plastic strain increase in the substrate. With further increase of the indentation depth, the values of the equivalent plastic strain in the film, both maximum and those in the nearby regions, remain at the same level as during stage II, although the deformed region extends parallel to the surface of the sample. For high indentation depths (stage I), the plastic deformed region of the substrate enlarges and the maximum value of the equivalent plastic strain in the substrate increases.

The mechanical behaviour of composites, where the film is harder than the substrate, can be described during stage II by a simple linear model (Eq. (10)), which describes the evolution of H_C/H_S *versus* t/h_c, within the range $1 < t/h_c < 6$.

The k_1 parameter of Eq.10 can be used as a measure of the relative hardness of the film (*i.e.* of the H_F/H_S ratio). Consequently, the H_F/H_S ratio can be expressed by a simple linear equation (Eq. (14)), as a function of the k_1 parameter. The evolution of the ratio H_F/H_S can be

more accurately expressed by a second order polynomial function of the k_1 parameter (Eq. (15)). Both equations are valid within the range $1 < t/h_c < 6$.

Acknowledgements

This research is sponsored by FEDER funds through the programme COMPETE–*Programa Operacional Factores de Competitividade*–and by national funds through FCT–*Fundação para a Ciência e a Tecnologia* –, under the project PEst-C/EME/UI0285/2011.

References

[1] J.V. Fernandes, A.C. Trindade, L.F. Menezes, A. Cavaleiro, Influence of substrate hardness on the response of W–C–Co-coated samples to depth-sensing indentation, Journal of Materials Research 15 (2000) 1766–1772.
[2] M. Lichinchi, C. Lenardi, J. Haupt, R. Vitali, Simulation of Berkovich nanoindentation experiments on thin films using finite element method, Thin Solid Films 312 (1998) 240–248.
[3] A.-C. Fisher-Cripps, Nanoindentation, second ed., Springer-Verlag, New York, 2004.
[4] C. Gamonpilas, E.P. Busso, On the effect of substrate properties on the indentation behaviour and hardness measurements of coated systems, Materials Science and Engineering: A 380 (2004) 52–61.
[5] I. Manika, J. Maniks, Effect of substrate hardness and film structure on indentation depth criteria for film hardness testing, Journal of Physics D: Applied Physics 41 (2008) 074010 (6 pp).
[6] J.V. Fernandes, L.F. Menezes, A.C. Trindade, The coated surface hardness: a kinematic model, Thin Solid Films 335 (1998) 153–159.
[7] J.M. Antunes, A. Cavaleiro, L.F. Menezes, M.I. Simoes, J.V. Fernandes, Ultra-microhardness testing procedure with Vickers indenter, Surface and Coatings Technology 149 (2002) 27–35.
[8] J.M. Antunes, J.V. Fernandes, L.F. Menezes, Three-dimensional numerical simulation of Vickers indentation tests, International Journal of Solids and Structures 43 (2006) 784–806.
[9] J.M. Antunes, L.F. Menezes, J.V. Fernandes, Influence of Vickers tip imperfection on depth sensing indentation tests, International Journal of Solids and Structures 44 (2007) 2732–2747.
[10] B. Jönsson, S. Hogmark, Hardness measurements of thin films, Thin Solid Films 114 (1984) 257–269.
[11] J. Lesage, D. Chicot, A. Pertuz, P.-Y. Jouan, N. Horny, A. Soom, A model for hardness determination of thin coatings from standard micro-indentation tests, Surface and Coatings Technology 200 (2005) 886–889.
[12] A.K. Bhattacharya, W.D. Nix, Analysis of elastic and plastic deformation associated with indentation testing of the thin films on substrates, International Journal of Solids and Structures 24 (1988) 1287–1298.
[13] H.L. Wang, M.J. Chiang, M.H. Hon, Determination of thin film hardness for a film/substrate system, Ceramics International 27 (2001) 385–389.
[14] A.M. Korsunsky, M.R. McGurk, S.J. Bull, T.F. Page, On the hardness of coated systems, Surface and Coatings Technology 99 (1998) 171–183.
[15] A. Iost, R. Bigot, Hardness of coatings, Surface and Coatings Technology 165 (1996) 117–120.
[16] Ichimura, F.M. Rodriguez, A. Rodrigo, The composite and film hardness of TiN coatings prepared by cathodic arc evaporation, Surface and Coatings Technology 127 (2000) 138–143.
[17] A. Iost, D. Najjar, R. Hellouin, Modelling of the Vickers hardness of paint coatings deposited on metallic substrates, Surface and Coatings Technology 165 (2003) 126–132.
[18] W.C. Oliver, G.M. Pharr, An improved technique for determining hardness and elastic-modulus using load and displacement sensing indentation experiments, Journal of Materials Research 7 (1992) 1564–1583.
[19] L.F. Menezes, C. Teodosiu, Three-dimensional numerical simulation of the deep-drawing process using solid finite elements, Journal of Materials Processing Technology 97 (2000) 100–106.
[20] M.C. Oliveira, J.L. Alves, L.F. Menezes, Algorithms and strategies for treatment of large deformation frictional contact in the numerical simulation of deep drawing process, Archives of Computational Methods in Engineering 15 (2008) 113–162.
[21] N.A. Sakharova, J.V. Fernandes, J.M. Antunes, M.C. Oliveira, Comparison between Berkovich, Vickers and conical indentation tests: A three-dimensional numerical simulation study, International Journal of Solids and Structures 46 (2009) 1095–1104.
[22] J.V. Fernandes, D.M. Rodrigues, L.F. Menezes, M.F. Vieira, A modified swift law for prestrained materials, International Journal of Plasticity 14 (1998) 537–550.
[23] D. Chicot, J. Lesage, Absolute hardness of films and coatings, Thin Solid Films 254 (1995) 123–130.
[24] I. Manika, J. Maniks, Characteristics of deformation localization and limits to the microhardness testing of amorphous and polycrystalline coatings, Thin Solid Films 208 (1992) 223–227.
[25] X. Cai, H. Bangert, Hardness measurements of thin films-determining the critical ratio of depth to thickness using FEM, Thin Solid Films 264 (1995) 59–71.
[26] R. Saha, W.D. Nix, Effects of the substrate on the determination of thin film mechanical properties by nanoindentation, Acta Materialia 50 (2002) 23–38.
[27] N.G. Chechenin, J. Bottiger, J.P. Krog, Nanoindentation of amorphous aluminium-oxide films I. The influence of the substrate on the plastic properties, Thin Solid Films 261 (1995) 219–227.
[28] J. Chen, S.J. Bull, On the factors affecting the critical indenter penetration for measurement of coating hardness, Vacuum 83 (2009) 911–920.
[29] E. Le Bourhis, P. Goudeau, M.H. Staia, E. Carrasquero, E.S. Puchi-Cabrera, Mechanical properties of hard AlCrN-based coated substrates, Surface and Coatings Technology 203 (2009) 2961–2968.
[30] P.K.P. Rupa, P.C. Chakraborti, S.K. Mishra, Mechanical and deformation behaviour of titanium diboride thin films deposited by magnetron sputtering, Thin Solid Films 517 (2009) 2912–2919.
[31] S.K. Mishra, P.K.P. Rupa, L.C. Pathak, Surface and nanoindentation studies on nanocrystalline titanium diboride thin film deposited by magnetron sputtering, Thin Solid Films 515 (2007) 6884–6889.
[32] L. Yate, J.C. Caicedo, A. Hurtado Macias, F.J. Espinoza-Beltrán, G. Zambrano, J. Muñoz-Saldaña, P. Prieto, Composition and mechanical properties of AlC, AlN and AlCN thin films obtained by r.f. magnetron sputtering, Surface and Coatings Technology 203 (2009) 1904–1907.
[33] A. Kumar, K.Y. Zeng, Measurement of hardness of ultra-thin films by the first derivation of load-displacement curve from nanoindentation data, International Journal of Modern Physics B 24 (2010) 256–266.